# Interfacial modification to improve inverted polymer solar cells

**Steven K. Hau,[a] Hin-Lap Yip,[a] Orb Acton,[a] Nam Seob Baek,[a] Hong Ma[a] and Alex K.-Y. Jen*[ab]**

***Received 12th May 2008, Accepted 14th August 2008***
***First published as an Advance Article on the web 1st October 2008***
**DOI: 10.1039/b808004f**

We report improved device performance of poly(3-hexylthiophene) (P3HT) and [6,6]phenyl $C_{61}$ butyric acid methyl ester (PCBM)-based inverted bulk-heterojunction (BHJ) solar cells through the modified interface of the $TiO_2$/BHJ with a series of carboxylic acid functionalized self-assembled monolayers (SAMs). The SAMs reduce the series resistance and improve the shunt resistance of the cell leading to increased fill factor and photocurrent density. Different aspects of device improvement can be affected depending on the nature of the SAMs. Modification with a $C_{60}$-SAM shows the largest enhancement leading to a 35% improvement ($\eta = 3.78\%$) over unmodified inverted devices ($\eta = 2.80\%$). This SAM serves multiple functions to affect the photoinduced charge transfer at the interface to reduce the recombination of charges, passivation of inorganic surface trap states, improve the exciton dissociation efficiency at the polymer/$TiO_2$ interface as well as a template to influence the overlayer BHJ distribution of phases, morphology and crystallinity leading to better charge selectivity and improved solar cell performance.

## Introduction

Organic photovoltaic devices have attracted considerable interest as promising low-cost, solution processable alternatives to inorganic-based photovoltaic devices.[1,2] The power conversion efficiency of polymer : fullerene based bulk-heterojunction devices has reached as high as ~5%. The high perfomance was achieved through the optimization of phase segregation in the blend and the development of new materials to allow better p–n interfaces and balanced hole and electron charge transport.[3–7] Until recently, most of the cells studied are based on the conventional device architecture which consists of a poly(3,4-ethylenedioxythiophene) : poly(styrenesulfonate) (PEDOT : PSS) hole-transporting layer and a bulk-heterojunction layer sandwiched between a high work function, hole collecting conducting transparent metal oxide electrode and a low work function, electron collecting metal electrode. However, the low work function metal electrode in this device geometry can be easily oxidized in air leading to deterioration in performance. To address this problem, a new device architecture using a titanium oxide or zinc oxide buffer layer between the organic active layer and the Al electrode has been used as a hole blocking and oxygen barrier layer to improve the device stability.[8–11] The device performance can be further improved by the modification of the metal oxide/metal interface using a self-assembled monolayer.[12,13]

Another way to circumvent this problem is to develop new device architectures that enable the use of a more air stable, high work function metal as the back electrode. Recently, inverted device geometries using high work function metals (Ag, Au) as the hole collecting electrode and metal oxides ($TiO_x$, ZnO) as the electron collecting contact have been reported.[14–19] We have already demonstrated improved ambient device stability using this inverted device architecture which retains over 80% of its original conversion efficiency after 40 days exposure to the atmosphere.[20] Besides the advantage of using a less air-sensitive electrode, the inverted device geometry avoids the need for using PEDOT : PSS at the ITO interface which has been shown to degrade performance due to chemical instabilities at the interface.[21] In addition, high work function metals offers the possibility for using non-vacuum techniques such as lamination or printing to deposit the top electrode.[22,23] Another advantage of the inverted device geometry is that if an n-type metal oxide is utilized with a bulk-heterojunction blend, the metal oxide can provide additional interfaces for exciton dissociation which can lead to an increase in photocurrent generation.[19] However, compared to the conventional device architecture, the inverted structures tend to have lower fill factors and photocurrent densities due to the un-optimized morphology of the bulk-heterojunction and poor charge selectivity at the electrode contact interfaces.[16,18]

The balanced charge transport and bulk resistance in each layer of an organic solar cell is extremely important to minimize charge recombination which will lead to the loss of performance.[24–27] The resistance in each layer must be minimized not only in the active layers, but also at the interfaces between layers. Appropriate electrical contacts between interfaces are important in order to determine the short-circuit current density ($J_{sc}$), open-circuit voltage ($V_{oc}$), and fill factor (FF) device characteristics of a solar cell. An ideal solar cell device should have low series resistance ($R_s$) and high shunt (parallel) resistance ($R_{sh}$) in order to optimize the device performance characteristics mentioned above. The series resistance reflects the ohmic loss in the entire device which is from a combination of the contact resistance and charge transfer rate at the interface as well as the bulk resistance of the active material. The shunt resistance reflects the loss of

[a]*Department of Materials Science and Engineering, University of Washington, Seattle, WA, 98195, USA. E-mail: ajen@u.washington.edu.; Fax: (+1) 206-543-3100; Tel: (+1) 206-543-2626*
[b]*Department of Chemistry, University of Washington, Seattle, WA, 98195, USA*

charge carriers due to current leakage pathways and recombination of charges in the bulk or at the interfaces.

One potential approach to simultaneously improve the morphology and charge selectivity of the inverted devices is to modify the interface between the inorganic and organic layer with a self-assembled monolayer (SAM). SAMs have been shown to significantly change the interfacial properties of various oxide and metallic surfaces. They can be used to improve adhesion, compatibility, and charge transfer properties at the interface to reduce back charge recombination. In addition, they can also be used to control the upper layer growth mode and distribution of phases, passivate inorganic surface trap states, and shift the interfacial energy offset between donor–acceptor materials.[28–33] However, the majority of the work using SAMs to modify the interface of organic solar cells are centered around dye-based carboxylic acids on $TiO_2$ for dye-sensitized solar cells or for inorganic–organic heterojunction cells.[34,35] There have been only a few attempts to use them to modify the interface of organic bulk-heterojunction cells.[31]

$TiO_2$ has been shown to be a good hole blocking and electron selective contact in inverted solar cells.[18] The lowest unoccupied molecular orbital (LUMO) and highest occupied molecular orbital (HOMO) of $TiO_2$ have been reported to be −4.4 eV and −7.6 eV, respectively.[36] This allows $TiO_2$ to function as a good interfacial layer between ITO and the bulk-heterojunction blend for inverted solar cell devices. Here we demonstrate the improved performance of P3HT : PCBM-based inverted bulk-heterojunction solar cells through the appropriate SAM modification on the electron collecting $TiO_2$ interface. The improved device performance is due to the reduction of series resistance and improved shunt resistance of the cell which can be attributed to the improvement of the following three aspects: 1) reduction of the contact resistance between the inorganic $TiO_2$ layer and active organic layer by passivation of surface trap states; 2) enhancement of the electronic coupling between the inorganic $TiO_2$ and active organic layer to mediate better forward charge transfer and reduce back charge recombination at the interface, and 3) affect the upper organic layer growth mode and morphology. We show that different aspects of device improvement can be affected depending on the nature of the SAMs.

## Experimental

### Materials

Regioregular poly(3-hexylthiophene) (P3HT) was purchased from Rieke Metals, Inc. and was used as received without further purification. The [6,6]phenyl $C_{61}$ butyric acid methyl ester (PCBM) was purchased from American Dye Source Inc. (99.0% purity), and was used as received without further purification.

Other chemicals were purchased from Aldrich and used as received unless otherwise specified. 2,2′:5′,2‴-Terthiophene-5-carboxylic acid was synthesized following a method similar to the reported one.[37] $^1$H NMR spectra (300 MHz) were recorded on a Bruker-300 FT NMR spectrometer with tetramethylsilane (TMS) as internal reference. Elemental analyses were determined at QTI (Whitehouse, NJ). ESI-MS spectra were obtained on a Bruker Daltonics Esquire Ion Trap Mass Spectrometer.

For the synthesis of $C_{60}$-substituted benzoic acid (Scheme 1), a mixture of 4-carboxybenzaldehyde (0.210 g, 1.40 mmol), $C_{60}$ (0.202 g, 0.28 mmol), and *N*-methylglycine (0.125 g, 1.40 mmol) in chlorobenzene (60 mL) was refluxed overnight under a nitrogen atmosphere. The solvent was removed by rotary evaporation under reduced pressure. The crude product was purified by silica gel column chromatography with toluene to toluene–THF (2 : 1) as the eluents to afford a brown-yellow solid (0.238 g, 95%). $^1$H NMR (300 MHz, DMSO-$d_6$): $\delta$ 2.20 (s, 3H), 6.65 (s, 1H), 6.89 (s, 2H), 8.03 (d, $J = 8.4$ Hz, 2H), 8.15 (d, $J = 8.4$ Hz, 2H), 10.12 (s, 1H). $C_{70}H_{11}NO_2$: calcd C 93.64, H 1.23, N 1.56; found C 93.45, H 1.31, N 1.62%. ESI-MS (*m*/*z*): calcd. 897.1; found 897.0.

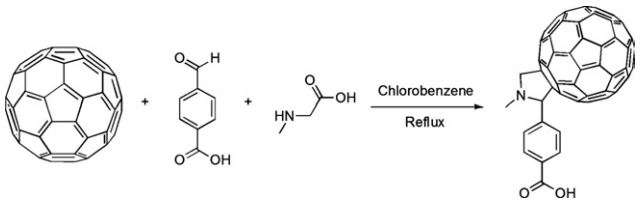


**Scheme 1** Synthesis of $C_{60}$-substituted benzoic acid.

### Device fabrication

To fabricate solar cells, ITO-coated glass substrates (15 Ω $\square^{-1}$) were cleaned in an ultrasonic bath with detergent, deionized (DI) water, acetone, and isopropyl alcohol and then dried under a $N_2$ stream. The substrates were then treated with oxygen plasma for 10 min. Titanium isopropoxide diluted in n-butyl alcohol was spun onto ITO at 3000 rpm (~40–50 nm). The films were annealed at 450 °C for 30 min to allow the growth of the crystalline anatase regions. The different monolayers were formed by immersing the sample in 0.1 mM solutions of either $C_{60}$, terthiophene, benzoic, or lauric acid in THF–ethanol (1 : 1) overnight. Samples were annealed at 140 °C for 20 min under $N_2$ to promote the chemical bonding of the SAM to the $TiO_2$ surface. After, the samples were sonicated in THF–ethanol for 5 min to remove any physically absorbed SAM molecules. The substrates were then transferred into an argon-filled glove box. The active layer was spun from a 40 mg mL$^{-1}$ solution of P3HT : PCBM (1 : 0.8 by weight) in 1,2-dichlorobenzene at 900 rpm for 60 s in an argon-filled glove box. The film was allowed to slowly dry in a covered Petri dish as described by Li *et al.*[4] and then thermally annealed at 150 °C for 10 min in the glove box. PEDOT : PSS (Baytron 4083) diluted with isopropyl alcohol and n-butyl alcohol was spun onto the active layer and annealed at 120 °C for 10 min under nitrogen before a second PEDOT : PSS (~30–40 nm) layer was spun on top and again annealed at 120 °C for 10 min under nitrogen. To complete the device structure, a 100 nm silver electrode was thermally evaporated (~$10^{-6}$ Torr) on top. Top contact organic field effect transistors (OFETs) and capacitance–voltage (*C*–*V*) samples (prepared on the same substrate as OFET) as well as X-ray diffraction samples were fabricated on heavily n-doped silicon substrates with a 300 nm thick thermally grown $SiO_2$ dielectric (from Montco Silicon Technologies, Inc.). Procedures for $TiO_2$, self assembly of $C_{60}$ molecules, and active layer preparation were performed in the same way as the solar cell fabrication. Pristine P3HT and PCBM films were fabricated by spin-coating 1 wt% solution in

 

1,2-dichlorobenezne and chloroform and annealed at 150 °C for 10 min, respectively. Interdigitated source and drain electrodes ($W = 9000$ μm, $L = 90$ μm, $W/L = 100$) for OFETs and $C$–$V$ samples ($D = 1$ mm) were defined by evaporating a 50 nm thick gold film through a shadow mask.

### Device characterization

The $J$–$V$ characteristics of the solar cells were tested in air using a Keithley 2400 source measurement unit and an Oriel xenon lamp (450 W) coupled with an AM1.5 filter was used as the light source. The light intensity was calibrated with a calibrated standard silicon solar cell with a KG5 filter which is traced to the National Renewable Energy Laboratory and a light intensity of a 100 mW $cm^{-2}$ was used in all the measurements in this study. The series resistance and parallel resistance were calculated from the inverse of the slope of the $J$–$V$ curve near 1 V and 0 V, respectively, under illumination. AFM images under tapping mode were taken on a Veeco multimode AFM with a Nanoscope III controller. X-Ray diffraction measurements were performed on a Bruker D8 X-ray diffractometer using an accelerating voltage of 40 kV and a Cu-K$\alpha$ source. OFET characterization was carried out in the dark under vacuum ($\sim 10^{-5}$ Torr) using a Keithley 2400 source measurement unit and a Keithley 6430 sub-femtoamp remote sourcemeter unit. $C$–$V$ measurements were performed from −35 V to 35 V in the dark under vacuum ($\sim 10^{-5}$ Torr) using an Agilent 4192A impedance analyzer.

## Results and discussion

The structure of the inverted polymer solar cells and the different types of SAMs employed in this study are shown in Fig. 1. The $TiO_2$ surface was characterized by taking multiple advancing contact angle measurements from various locations on the substrates modified with and without the SAMs. Table 1 shows the average contact angles with ±3° uncertainty on the various SAM modified surfaces. Without SAM modification, the surface of $TiO_2$ after oxygen plasma had a low wetting angle to DI water (~5°) showing a hydrophilic surface. The formation of the SAMs was confirmed from the results showing an increase in contact angle (hydrophobic surface) after surface modification. The modified SAM surface was also characterized by atomic force microscopy (AFM, Fig. 2) showing negligible differences between the unmodified surface and the modified SAM surfaces.

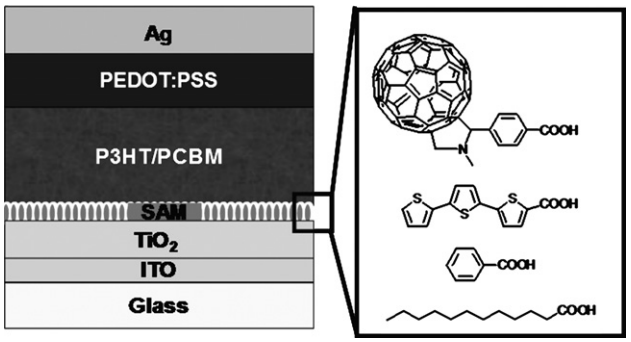


**Fig. 1** Device architecture of the inverted polymer solar cell with the different self-assembled molecules used to modify the $TiO_2$ surface. (Right side, top to bottom) $C_{60}$ based SAM, terthiophene SAM, benzoic acid SAM, and lauric acid SAM.

**Table 1** Summary of the average device performance of inverted P3HT : PCBM bulk heterojunction solar cells with and without carboxylic acid self-assembled monolayer modification (performance averaged over 40 devices)

| SAM | Contact angle/° | $V_{oc}$/V | $J_{sc}$/mA $cm^{-2}$ | FF (%) | $\eta$ (%) | $R_s$/Ω $cm^2$ | $R_{sh}$/Ω $cm^2$ |
|---|---|---|---|---|---|---|---|
| None | ~5 | 0.61 | 9.80 | 46.9 | 2.8 | 13 | 380 |
| $C_{60}$ | 63 | 0.62 | 10.6 | 57.2 | 3.8 | 2.4 | 1010 |
| Terthiophene (TT) | 56 | 0.60 | 10.0 | 56.2 | 3.4 | 3.5 | 880 |
| Benzoic acid (BA) | 45 | 0.60 | 10.5 | 50.2 | 3.2 | 2.7 | 580 |
| Lauric acid (LA) | 83 | 0.61 | 9.92 | 49.5 | 3.0 | 2.6 | 440 |

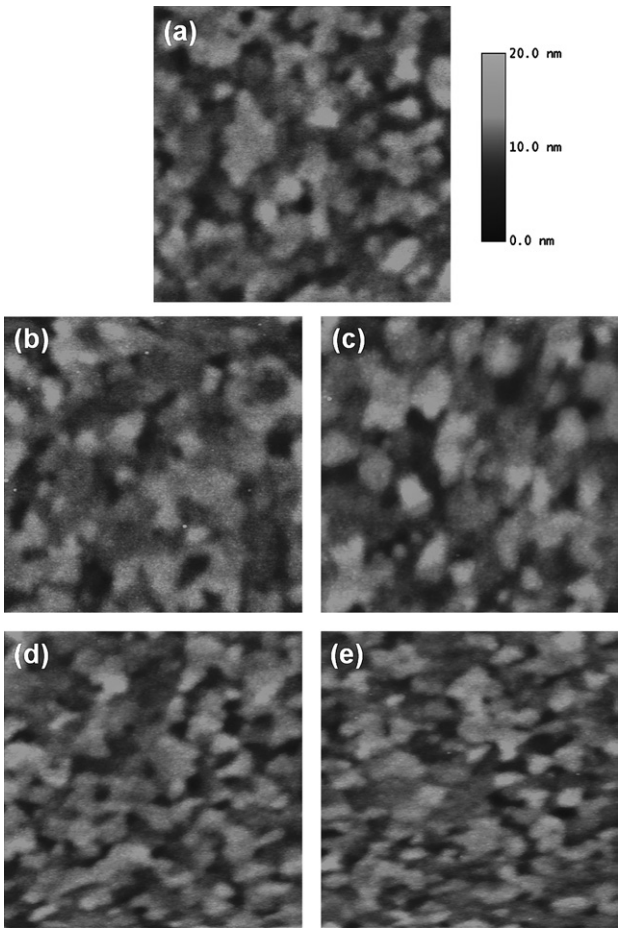


**Fig. 2** AFM images of the $TiO_2$ surface modified with SAMs. (a) Unmodified $TiO_2$ surface, (b) $C_{60}$-SAM, (c) TT-SAM, (d) BA-SAM, (e) LA-SAM. All AFM image scans are 2 μm × 2 μm.

### Bulk-heterojunction device performance

Fig. 3a shows the $J$–$V$ characteristics for the inverted bulk-heterojunction cells with and without modification with carboxylic acid SAMs under AM1.5 illumination. From the inset of Fig. 3a, the log plot of $J$–$V$, the modification of the surface of $TiO_2$ with

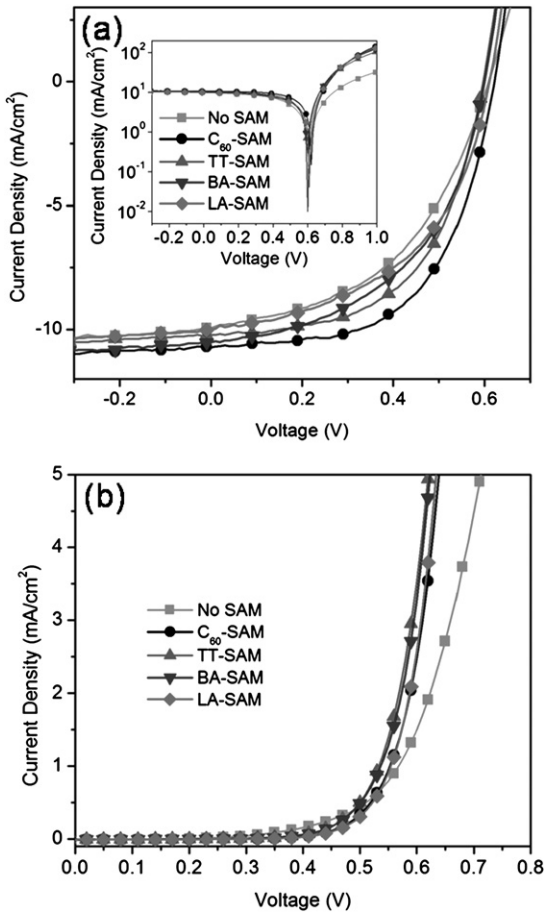


**Fig. 3** The current density–voltage ($J$–$V$) characteristics of the inverted P3HT : PCBM bulk heterojunction solar cells modified with and without self-assembled monolayers: (a) under AM1.5 illumination (100 mW $cm^{-2}$) (inset: plot of illuminated $J$–$V$ curve in log scale) and (b) in the dark.

SAMs shows almost one order of magnitude higher in current density at 1 V compared to the device without any SAM modification. This indicates that the SAM reduces the series resistance of the cell which is attributed to better compatibility and removal of surface trap states on the $TiO_2$ surface.[30,38] Furthermore, the dark $J$–$V$ plot in Fig. 3b reveals similar improvement in diode performance from the SAM modified devices. A summary of the average device performance with and without monolayer modification is given in Table 1. The devices without SAM modification have an average power conversion efficiency ($\eta$) of 2.8% with a $J_{sc} = 9.80$ mA $cm^{-2}$, a $V_{oc} = 0.61$ V and a FF = 46.9 which are comparable to the reported literature values.[16,18] SAM modified devices show overall improvements in series resistance ($R_s$) from 13 Ω $cm^2$ to 3–4 Ω $cm^2$ and shunt resistance ($R_{sh}$) compared to devices without modification. The series and shunt resistances are calculated from the inverse gradient of the $J$–$V$ curve at 1 V and at the short circuit current density under illumination. The LA-SAM shows a slight improvement of $\eta$ to 3.0 %. The $J_{sc}$ and $V_{oc}$ values remain similar to those of devices without a monolayer; however, the FF increases slightly to 49.5 which is most likely attributed to the reduced surface traps leading to better contact. Modification with the BA-SAM shows further enhancement in performance having $\eta = 3.2\%$. The FF is similar to that of devices modified with LA-SAM. The $V_{oc}$ value decreases slightly, but is compensated by the increase in $J_{sc}$ to improve the overall performance. The improved $J_{sc}$ is attributed to BA-SAM improving the interfacial electron transfer by removing the trap states at the interface of the $TiO_2$ layer as described by Moser *et al.*[38] When the surface of $TiO_2$ is modified with an electroactive functional group such as terthiophene or $C_{60}$, the average efficiencies are further improved by 0.6% and 1.0%, respectively, compared to devices without a monolayer. The FF of the TT-SAM and $C_{60}$-SAM devices show a dramatic increase to 56.2 and 57.2, respectively, compared to the device without SAM modification indicating that the electroactive groups on the SAM help to improve charge selectivity and reduce the charge recombination losses at the interface. In addition to helping passivate surface traps to improve the contact resistance, TT-SAM and $C_{60}$-SAM may also be promoting photoinduced charge transfer at the interface. $C_{60}$-SAM shows the lowest $R_s$ (~2.4 Ω $cm^2$) and the highest $R_{sh}$ (~1010 Ω $cm^2$) leading to average device efficiencies of 3.8%.

## Photoinduced charge transfer

To investigate the photo-induced charge transfer properties at the inorganic/SAM/organic interface, heterojunction devices with and without SAM modification on $TiO_2$ and pristine P3HT were fabricated. Since the only exciton dissociation site in this heterojunction structure is at the n-type $TiO_2$/p-type P3HT interface, the effect of the SAM on the exciton dissociation efficiency can be independently studied. The $J$–$V$ plot of the heterojunction devices under AM1.5 illumination is given in Fig. 4a. The plot shows that LA-SAM and BA-SAM do not have a large effect on the device performance. However, TT-SAM and $C_{60}$-SAM result in improvements in all the device characteristics. Table 2 summarizes the device performance of the SAM modified heterojunction devices. TT-SAM and $C_{60}$-SAM, which are both electroactive, show improvements in fill factor and photocurrent density which confirms that photoinduced charge transfer at the interface plays a role in preventing charge back recombination at the $TiO_2$ interface. $C_{60}$-SAM shows the largest improvement which is not surprising since the $C_{60}$ molecule has already been shown to be a very good electron acceptor (n-type) under illumination due to photoinduced electron transfer from polymer to $C_{60}$.[39] This photoinduced electron transfer from P3HT to the $C_{60}$-SAM in the heterojunction device explains why the blend P3HT : PCBM device also shows improved performance since in the blend device, both P3HT and PCBM can be located at that interface. The dark log $J$–$V$ characteristics of the heterojunction devices are given in Fig. 4b from which the diode rectification ratio at ±3 V is extracted.[40] Both the unmodified and LA-SAM showed similar rectification: ~$10^{-2}$. BA-SAM had improved rectification followed by TT-SAM. The $C_{60}$-SAM had the best rectification ratio of ~$10^{-4}$ which indicates that it serves as an effective hole blocking layer.

## Morphology

To investigate the effect of the monolayers on the overlayer film formation, AFM was used to track the changes prior to and after

 

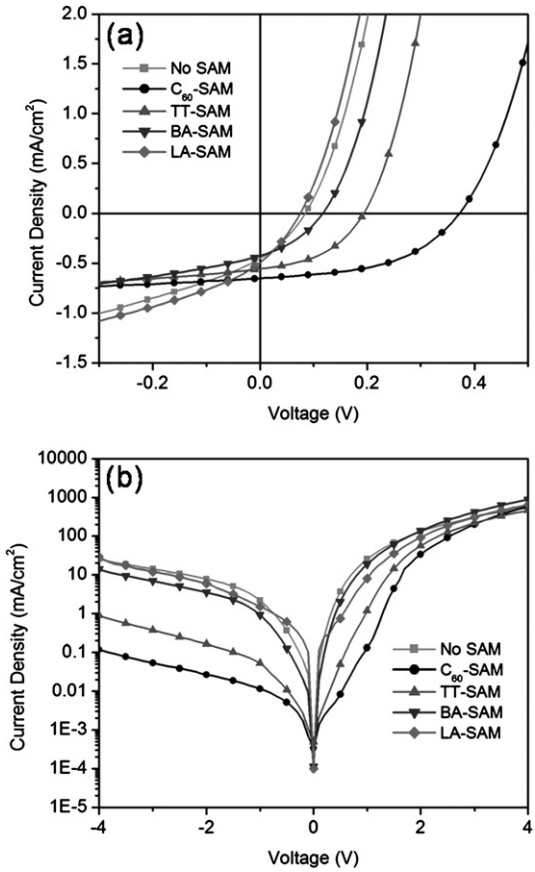


**Fig. 4** The current density–voltage ($J$–$V$) characteristics of the inverted P3HT : $TiO_2$ heterojunction solar cells modified with and without self-assembled monolayers under AM1.5 illumination (100 mW $cm^{-2}$) plotted on a linear scale (a) and in the dark plotted on a log scale (b).

**Table 2** Summary of the average device performance of inverted P3HT : $TiO_2$ heterojunction solar cells with and without carboxylic acid self-assembled monolayer modification (performance averaged over 40 devices)

| SAM | $V_{oc}$/V | $J_{sc}$/mA $cm^{-2}$ | FF (%) | $\eta$ (%) | Rectification ratio |
|---|---|---|---|---|---|
| None | 0.08 | 0.45 | 31.5 | 0.01 | $4 \times 10^{-2}$ |
| $C_{60}$ | 0.37 | 0.65 | 49.1 | 0.12 | $3 \times 10^{-4}$ |
| Terthiophene (TT) | 0.19 | 0.56 | 44.1 | 0.05 | $2 \times 10^{-3}$ |
| Benzoic acid (BA) | 0.12 | 0.43 | 35.7 | 0.02 | $2 \times 10^{-2}$ |
| Lauric acid (LA) | 0.07 | 0.49 | 30.6 | 0.01 | $4 \times 10^{-2}$ |

annealing the blend films at 150 °C. AFM images in Fig. 5 show that the morphology of unannealed blend film surfaces with and without SAM layers have a very rough surface around ~5–6 nm rms. Upon annealing at 150 °C, the surface roughness of all the devices increase slightly to ~6–8 nm rms. The device without SAM modification increased from 5.7 nm rms to 6.3 nm rms while the $C_{60}$-SAM modified device increased from 6.1 nm rms to 7.9 nm rms after annealing. These results are consistent with prior reports from Li *et al.* who suggested that the slow drying rate using 1,2-dichlorobenzene as the solvent allows the P3HT

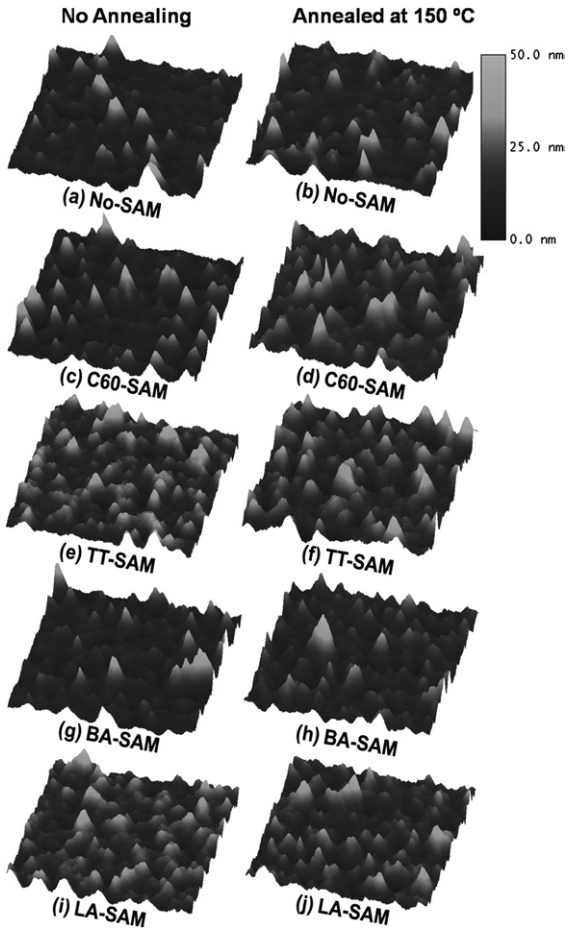


**Fig. 5** AFM images of P3HT : PCBM spin-coated on $TiO_2$ surfaces modified with and without SAMs before and after annealing at 150 °C. Unmodified $TiO_2$ surface: (a) no annealing, (b) annealed at 150 °C. Modified with $C_{60}$-SAM: (c) no annealing, (d) annealed at 150 °C. Modified with TT-SAM: (e) no annealing, (f) annealed at 150 °C. Modified with BA-SAM: (g) no annealing, (h) annealed at 150 °C. Modified with LA-SAM: (i) no annealing, (j) annealed at 150 °C. All AFM image scans are 2 μm × 2 μm.

chains to self-organize leading to better ordering.[4] Indeed, the $C_{60}$-SAM modified devices showed a much rougher surface morphology compared to the others. The increase in surface roughness has been correlated to better ordering of the P3HT chains in blend films leading to better performing devices; however, it does not necessarily give quantitative information regarding its crystallinity and can only be an indirect method to determine performance of devices.

## X-Ray diffraction

To study the effect of the SAM modification on the overlayer crystallinity of the P3HT : PCBM blend, X-ray diffraction samples were prepared. Fig. 6 shows the X-ray diffraction spectra of the bulk-heterojunction blend before and after annealing at 150 °C on devices with and without SAMs. Fig. 6(b) shows the diffraction peaks of P3HT (100) on devices without a monolayer before and after thermal annealing. Fig. 6(b) shows

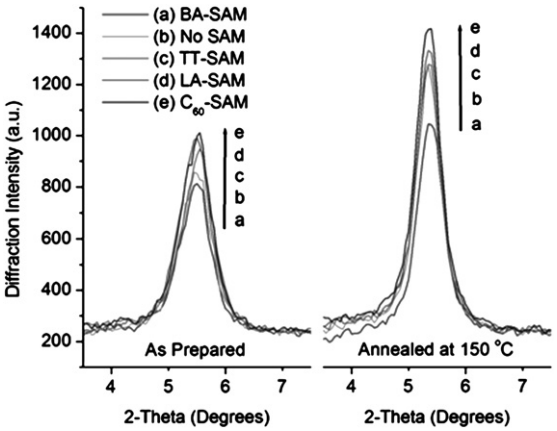


**Fig. 6** X-Ray diffraction spectra of the P3HT (100) peaks before and after thermal annealing at 150 °C on bulk heterojunction devices modified with and without SAMs.

an increase in intensity after annealing indicating better P3HT ordering. The P3HT diffraction intensity of devices modified with BA-SAM are lower (Fig. 6(a)) than those without a monolayer showing a negative influence on the overlayer crystallinity implying that improved device performance from BA-SAM is attributed mainly to the improved charge transfer and lower contact resistance at the interface. TT-SAM devices show an increase in P3HT diffraction signal (Fig. 6(c)). This improvement in crystallinity in addition to the improved charge transfer and lower contact resistance leads to better performing devices. The device performance of LA-SAM is poor even though it shows a large affect on P3HT ordering (Fig. 6(d)). The improved order is due to the long alkyl chain SAM interacting with P3HT to help order the P3HT chains.[41] The slight improvement in device performance is due to the improved crystallinity of the bulk blend which lowers the series resistance of the device. The improvement, however, is not likely to be due to improved charge transfer at the interface since lauric acid is not electroactive and will act as a physical barrier that affects the electronic coupling between the polymer and $TiO_2$. Devices modified with $C_{60}$-SAM show the largest increase in the diffraction signal (Fig. 6(e)) both before and after annealing, confirming that it can affect the overlayer crystallinity and morphology. The combined improvements in P3HT crystallinity, contact resistance by passivating surface traps, and photoinduced charge transfer to reduce back charge recombination are the reasons for the high performance in the $C_{60}$-SAM modified devices.

### *C–V* and FET measurements

To further understand the effect of the $C_{60}$-SAM on the interface between the organic active and inorganic $TiO_2$ layer, organic field effect transistors (OFET) and capacitance–voltage (*C–V*) measurements were performed. It has been shown that characterizing blend films of P3HT : PCBM using OFETs and *C–V* can give information regarding the distribution and vertical concentration gradients of the organic materials close to the interface.[42] The transport properties in OFETs are generally determined by the first few nanometers of the active material close to the interface. If one of the two components of the blend

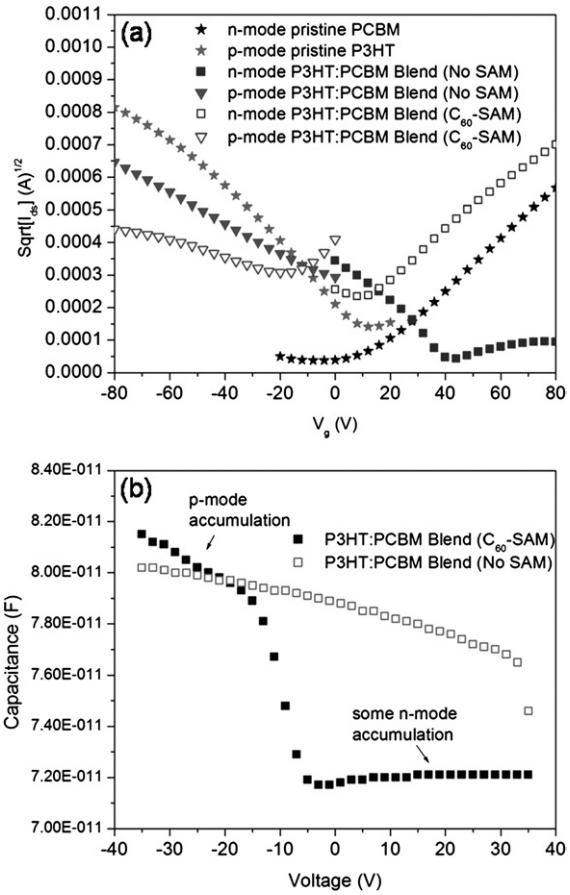


**Fig. 7** (a) Square roots of the measured transfer characteristics of OFETs prepared from the pristine P3HT, PCBM and blend films of P3HT : PCBM (weight ratio 1 : 0.8) with and without $C_{60}$-SAM modification at the $TiO_2$ interface. (b) Capacitance–voltage measurements of blend films of P3HT : PCBM (weight ratio 1 : 0.8) with and without $C_{60}$-SAM modification at the $TiO_2$ interface.

segregates towards the bottom interface, the charge carrier mobility should ideally reach its pristine value. OFETs were fabricated of the pristine films of P3HT and PCBM on a $TiO_2$/$SiO_2$/doped-Si substrate. The square roots of the transfer characteristics of the pristine films of P3HT and PCBM are given in Fig. 7a. The mobility is calculated from the slope of the line giving a hole mobility of $1.8 \times 10^{-4}$ $cm^2$ $V^{-1}$ $s^{-1}$ for P3HT and an electron mobility of $1.2 \times 10^{-4}$ $cm^2$ $V^{-1}$ $s^{-1}$ for PCBM. The blend film without SAM modification had a hole mobility of $4.1 \times 10^{-5}$ $cm^2$ $V^{-1}$ $s^{-1}$ and an electron mobility of $9.4 \times 10^{-6}$ $cm^2$ $V^{-1}$ $s^{-1}$. The higher hole mobility compared to electron mobility indicates that a higher concentration of P3HT is accumulated at the interface which is in agreement with previous reports of blend films cast from dichlorobenzene showing higher concentrations of P3HT near the bottom interface.[43] The blend film with $C_{60}$-SAM modification, however, had a hole mobility of $1.8 \times 10^{-5}$ $cm^2$ $V^{-1}$ $s^{-1}$ and an electron mobility of $1.0 \times 10^{-4}$ $cm^2$ $V^{-1}$ $s^{-1}$. In this case, the electron mobility is higher than the hole mobility confirming that more PCBM is accumulated at the interface. *C–V* measurements shown in Fig. 7b also indicate that the $C_{60}$-SAM facilitates the accumulation of PCBM to the bottom $TiO_2$ interface. The $C_{60}$-SAM modified devices show p-mode and

 

n-mode accumulation which is in agreement with what was found from the OFET measurements. Without SAM modification, the *C–V* shows higher capacitance under negative gate voltage implying a more p-mode accumulation at the interface. However, under positive gate voltage, no significant n-mode accumulation is observed. This proves that the $C_{60}$-SAM can help to nucleate PCBM to provide a better percolation conduction pathway of PCBM at the interface which improves the overall distribution of phases, morphology and crystallinity of the blend leading to better charge selectivity.

## Conclusions

In conclusion, we have found that modification of the interface between the inorganic $TiO_2$ and organic bulk-heterojunction layer with a SAM can improve the performance of inverted photovoltaic cells. Depending on the functionality of the SAM, it can help to improve the contact resistance and charge transfer at the interface as well as influence the overlayer distribution of phases, morphology and crystalline order. The $C_{60}$-SAM leads to a 35% improvement over unmodified $TiO_2$ inverted devices. This SAM serves multiple functions to affect the photoinduced charge transfer at the interface to reduce the recombination of charges, passivation of inorganic surface trap states, improve the exciton dissociation efficiency at the polymer/$TiO_2$ interface as well as acting as a template to influence the overlayer bulk-heterojunction distribution of phases and crystallinity leading to better charge selectivity. Understanding how to improve the interface resistance as well as the bulk-heterojunction resistance in a photovoltaic cell is critical to prevent recombination of charges that lead to losses in photovoltaic performance.

## Acknowledgements

This work was supported by the National Science Foundation's STC program under DMR-0120967 and the DOE "Future Generation Photovoltaic Devices and Process" program. A. K. Y. Jen thanks the Boeing-Johnson Foundation for the financial support. S. K. Hau and H. L. Yip thank the Intel Foundation Ph.D Fellowship. The authors would like to thank Prof. Fumio Ohuchi and Patrick Shamberger with their help with the XRD measurements.

## References

1 H. Hoppe and N. S. Sariciftci, *J. Mater. Res.*, 2004, **19**, 7.
2 S. Gunes, H. Neugebauer and N. S. Sariciftci, *Chem. Rev.*, 2007, **107**, 1324.
3 K. Kim, J. Liu, M. A. G. Namboothiry and D. L. Carroll, *Appl. Phys. Lett.*, 2007, **90**, 163511.
4 G. Li, V. Shrotriya, J. S. Huang, Y. Yao, T. Moriarty, K. Emery and Y. Yang, *Nat. Mater.*, 2005, **4**, 864.
5 W. L. Ma, C. Y. Yang, X. Gong, K. Lee and A. J. Heeger, *Adv. Funct. Mater.*, 2005, **15**, 1617.
6 J. Peet, J. Y. Kim, N. E. Coates, W. L. Ma, D. Moses, A. J. Heeger and G. C. Bazan, *Nat. Mater.*, 2007, **6**, 497.
7 W. Y. Wong, X. Z. Wang, Z. He, A. B. Djurisic, C. T. Yip, K. Y. Cheung, H. Wang, C. S. K. Mak and W. K. Chan, *Nat. Mater.*, 2007, **6**, 521.
8 J. Y. Kim, K. Lee, N. E. Coates, D. Moses, T. Q. Nguyen, M. Dante and A. J. Heeger, *Science*, 2007, **317**, 222.
9 K. Lee, J. Y. Kim, S. H. Park, S. H. Kim, S. Cho and A. J. Heeger, *Adv. Mater.*, 2007, **19**, 2445.
10 J. Y. Kim, S. H. Kim, H. H. Lee, K. Lee, W. Ma, X. Gong and A. J. Heeger, *Adv. Mater.*, 2006, **18**, 572.
11 J. Gilot, I. Barbu, M. M. Wienk and R. A. J. Janssen, *Appl. Phys. Lett.*, 2007, **91**, 113520.
12 H. L. Yip, S. K. Hau, N. S. Baek, H. Ma and A. K. Y. Jen, *Adv. Mater.*, 2008, **20**, 2376–2382.
13 H. L. Yip, S. K. Hau, N. S. Baek and A. K. Y. Jen, *Appl. Phys. Lett.*, 2008, **92**, 193313.
14 A. C. Arango, L. R. Johnson, V. N. Bliznyuk, Z. Schlesinger, S. A. Carter and H. H. Horold, *Adv. Mater.*, 2000, **12**, 1689.
15 Y. X. Liu, M. A. Summers, C. Edder, J. M. J. Frechet and M. D. McGehee, *Adv. Mater.*, 2005, **17**, 2960.
16 M. S. White, D. D. Olson, S. E. Shaheen, N. Kopidakis and D. S. Ginley, *Appl. Phys. Lett.*, 2006, **89**, 142517.
17 J. Owen, M. S. Son, Y. H. Yoo, B. D. Ahn and S. Y. Lee, *Appl. Phys. Lett.*, 2007, **90**, 033512.
18 C. Waldauf, M. Morana, P. Denk, P. Schilinsky, K. Coakley, S. A. Choulis and C. J. Brabec, *Appl. Phys. Lett.*, 2006, **89**, 233517.
19 G. K. Mor, K. Shankar, M. Paulos, O. K. Varghese and C. A. Grimes, *Appl. Phys. Lett.*, 2007, **91**, 152111.
20 S. K. Hau, H. L. Yip, N. S. Baek, J. Zou, K. O'Malley and A. K. Y. Jen, *Appl. Phys. Lett.*, 2008, **92**, 253301.
21 M. P. de Jong, L. J. van IJzendoorn and M. J. A. de Voigt, *Appl. Phys. Lett.*, 2000, **77**, 2255.
22 D. A. Bernards, T. Biegala, Z. A. Samuels, J. D. Slinker, G. G. Malliaras, S. F. Torres, H. D. Abruna and J. A. Rogers, *Appl. Phys. Lett.*, 2004, **84**, 3675.
23 W. J. Zeng, H. B. Wu, C. Zhang, F. Huang, J. B. Peng, W. Yang and Y. Cao, *Adv. Mater.*, 2007, **19**, 810.
24 T. Aernouts, W. Greens, J. Poortmans, P. Heremans, S. Borghs and R. Mertens, *Thin Solid Films*, 2002, **403**, 297.
25 C. Melzer, E. J. Koop, V. D. Mihailetchi and P. W. M. Blom, *Adv. Funct. Mater.*, 2004, **14**, 865.
26 B. Y. Ouyang, C. W. Chi, F. C. Chen, Q. F. Xi and Y. Yang, *Adv. Funct. Mater.*, 2005, **15**, 203.
27 C. J. Ko, Y. K. Lin, F. C. Chen and C. W. Chu, *Appl. Phys. Lett.*, 2007, **90**, 063509.
28 S. Khodabakhsh, B. M. Sanderson, J. Nelson and T. S. Jones, *Adv. Funct. Mater.*, 2006, **16**, 95.
29 N. R. Armstrong, C. Carter, C. Donley, A. Simmonds, P. Lee, M. Brumbach, B. Kippelen, B. Domercq and S. Yoo, *Thin Solid Films*, 2003, **445**, 342.
30 C. Goh, S. R. Scully and M. D. McGehee, *J. Appl. Phys.*, 2007, **101**, 114503.
31 J. S. Kim, J. H. Park, J. H. Lee, J. Jo, D.-Y. Kim and K. Cho, *Appl. Phys. Lett.*, 2007, **91**, 112111.
32 J. Kruger, U. Bach and M. Gratzel, *Adv. Mater.*, 2000, **12**, 447.
33 R. J. Kline, M. D. McGehee and M. F. Toney, *Nat. Mater.*, 2006, **5**, 222.
34 B. Oregan and M. Gratzel, *Nature*, 1991, **353**, 737.
35 N. Kudo, S. Honda, Y. Shmiazaki, H. Ohkita, S. Ito and H. Benten, *Appl. Phys. Lett.*, 2007, **90**, 183513.
36 M. Gratzel, *Nature*, 2001, **414**, 338.
37 J. Kagan, S. K. Arora and A. Ustunol, *J. Org. Chem.*, 1983, **48**, 4076.
38 J. Moser, S. Punchihewa, P. P. Infelta and M. Gratzel, *Langmuir*, 1991, **7**, 3012.
39 N. S. Sariciftci, L. Smilowitz, A. J. Heeger and F. Wudl, *Science*, 1992, **258**, 1474.
40 A. Hayakawa, O. Yoshikawa, T. Fujieda, K. Uehara and S. Yoshikawa, *Appl. Phys. Lett.*, 2007, **90**, 163517.
41 D. H. Kim, Y. Jang, Y. D. Park and K. Cho, *Langmuir*, 2005, **21**, 3203.
42 M. Morana, P. Koers, C. Waldauf, M. Koppe, D. Muehlbacher, P. Denk, M. Scharber, D. Waller and C. Brabec, *Adv. Funct. Mater.*, 2007, **17**, 3274.
43 Y. Kim, S. A. Choulis, J. Nelson, D. D. C. Bradley, S. Cook and J. R. Durrant, *Appl. Phys. Lett.*, 2005, **86**, 063502.